



Applications of modified Darcy law and nonlinear thermal radiation in bioconvection flow of micropolar nanofluid over an off centered rotating disk

Ying-Qing Song^a, Shan Ali Khan^b, Muhammad Imran^b, Hassan Waqas^b,
Sami Ullah Khan^c, M. Ijaz Khan^d, Sumaira Qayyum^e, Yu-Ming Chu^{f,g,*}

^a College of Science, Hunan City University, Yiyang 413000, PR China

^b Department of Mathematics, Government College University Faisalabad, 38000, Pakistan

^c Department of Mathematics, COMSATS University Islamabad, Sahiwal 57000, Pakistan

^d Department of Mathematics and Statistics, Riphah International University I-14, Islamabad 44000, Pakistan

^e Department of Mathematics, Quaid-I-Azam University 45320, Islamabad 44000, Pakistan

^f Department of Mathematics, Huzhou University, Huzhou 313000, PR China

^g Hunan Provincial Key Laboratory of Mathematical Modeling and Analysis in Engineering, Changsha University of Science & Technology, Changsha 410114, PR China

Received 31 January 2021; revised 8 March 2021; accepted 23 March 2021

KEYWORDS

Modified Darcy's law;
Micropolar nanofluid;
Rotating disk;
Thermal radiation;
Shooting technique

Abstract To improve the heat efficiency base fluids (water, engine oil, glycol), the interaction of nanoparticles (nanotubes, droplets, nanowires, metals and non-metals) into such traditional liquids is the most frequent mechanism and attained the researchers attention, especially in current decade. The nanofluid is a suspension of submerged solid particles in base fluids. The nano-materials con- veyed the applications in the field of nanotechnology, thermal engineering, industrial and bio- engineering. Following to such motivating applications in mind, current research reports the stag- nation point flow of radiative micropolar nanofluid over an off centered rotating disk with appli- cations of motile microorganisms. The novel dynamic of thermal radiation and activation energy are also incorporated. The appropriate transformations are utilized to reduce the partial differential equations into dimensionless forms. A numerical shooting scheme is used to obtain the approximate solution with MATLAB software. The effects of prominent parameter on velocity profile, nanofluid temperature, concentration of nanoparticles and microorganism profile are physically incorporated.

© 2021 THE AUTHORS. Published by Elsevier BV on behalf of Faculty of Engineering, Alexandria University. This is an open access article under the CC BY-NC-ND license (<http://creativecommons.org/licenses/by-nc-nd/4.0/>).

* Corresponding author.

E-mail address: chuyuming@zjhu.edu.cn (Y.-M. Chu).

Peer review under responsibility of Faculty of Engineering, Alexandria University.

<https://doi.org/10.1016/j.aej.2021.03.053>

1110-0168 © 2021 THE AUTHORS. Published by Elsevier BV on behalf of Faculty of Engineering, Alexandria University. This is an open access article under the CC BY-NC-ND license (<http://creativecommons.org/licenses/by-nc-nd/4.0/>).

1. Introduction

Owing to the extensive applications of nanofluids in the manufacturing field, thermal engineering and technological process, the study of nanofluids become a fascinating research area. Some dynamic applications of such materials include manufactures of polymers, gas generators, power engines, glass material, paper creating, wire illustration etc. Nanofluids are introduced as most source of energy with size less than 1–100 nm and uniformly distributed in the base fluid, such as water, oil, ethanol glycol. Such transmitted nanoparticles, particularly transition metals as well as metal oxides, significantly increase the thermal conductivity including its nanofluid, improved the absorption and convection parameters, and allow additional heat to be transferred. Improving the thermal requirements of fluids contributes to a higher degree of thermal unit connective movement. In order to improve the heat transport, the addition of chemicals to the operating fluids to change the thermal characteristics is a very interesting process. Towards this effect, a direction has been identified by an improvement in nanotechnology. Choi [1] initially explored the properties of nanofluid experimentally. Later on a number of investigations are performed to demonstrate the efficiency of asymmetric nanofluids. Buongiorno [2] explored two significant slip mechanism including thermophoresis diffusion and Brownian motion features. Zhu et al. [3] explored the heat transmission of nanofluids containing various nanoparticles within a parallel-plate channel. Geridönmez et al. [4] examined the convective flow of hybrid nanoparticles in backwards process channel with applications of standardized partial electromagnetic field. Ali et al. [5] described the improved thermal transport of Carreau nanofluids through an expanding wedge. Qureshi [6] investigated the heat transmission and entropy of continuous in Williamson nanofluid flow on the basis of essential symmetry. Mehta et al. [7] scrutinized the influence of a three-dimensional water composite nanoliquid material in a revolving device confined by two horizontally parallel platelets. The characterized the heat transmission frequency of the simultaneously embedding of triangle blades and porous discs in ring pipe was evaluated by Poursharif et al. [8]. Sreedevi et al. [9] examined the thermal consequences of Williamson nanoparticles stream over a wedge with utilization of carbon nanotubes. Thermally-hydraulic properties and efficiency of turbulent movement of numerous nanofluids in multiple conical dual pipe heat exchangers were mathematically observed by Khalil et al. [10]. Wen et al. [11] analyzed mixed transport ZnO and ethanol glycol hybrid nanofluid in a nano channels containing hydraulic sizes. Some more contributions of nanofluids flow can be seen in refs. [12–16]. Khan et al. [17] examined the heat and mass characteristics in third grade nanofluid in presence of variable reactive index.

“Activation energy” is the minimum quantity of energy needed to process the molecules and atoms in any chemical process and chemical reactions. The word activation energy was first used by Swedish mathematician Svante Arrhenius in 1889. Some substances or molecules behave together in the existence of specified quantities of energy. Activation energy is known to be dividing barrier among two energy systems. When this energy is exceeded, a chemical process will undergoes and subsequently chemical reaction enhanced. At an acceptable frequency for a chemical process, there is a large

number of an element or molecules with a computational energy processor equivalent to or similar to the activation energy. With Maxwell distribution, the atoms that can cross the barriers are those of greater energy than the barriers. The activation energy is indeed the length for the barrier. During this instance, we are ignoring the involvement of tunneling and the form of the barrier that defines the number of molecules with greater energy than the barrier that actually induces the response. This amount is defined as k_0 . Interestingly, the percentage of molecules with appropriate energy to response will depends on energy, which is why we are adding a pre-exponential temperature feature variable. This method is widely utilized in the estimation of rates, initially testing cross-sections. The analysis of binary chemical reaction through the boundary layer stream was introduced by Bestman [18] where heat and mass transport were examined through a porous medium using binary reaction and Arrhenius activation energy. Gotoh et al. [19] investigated the applications of activation energy in hydrocarbons chemisorptions throughout higher-performance titanium oxides providing interaction for silicone oxidation interlayer. Alwatban et al. [20] incorporated the slip mechanism and activation energy application in Eyring-Powell nanofluid flow numerically. Khan et al. [21] focused on the activation energy applications along with entropy generation in nanofluid flow. Bhatti et al. [22] inspected the applications in bioconvection in blood flow through anisotropically tapered arteries.

Bioconvection is an interesting process of materials associated with the swimming of microorganisms. The phenomenon of bioconvection performs a key role in the production of biochemical oils and meteorological applications including heated spring colonised through motile gyrotactic microorganisms termed as thermopil. Bioconvection implies the microstructural movement of fluid flow convection induced by density patterns associated with hydrodynamic momentum and primary investigated by Kuznetsov, [23]. The compilation of microorganisms (mammals and microbes) in primary fluids allows the bioconvection applications like natural reasons, for example light, gravitation, magnetic field as well as mechanical concentration (oxygen). Bioconvection can be utilized in a broad variety of applications including biomedical applications including biomicrosystems, pharmaceutical manufacturers, biopolymer synthesis, environmental protected applications, advanced fuel cell engineering, microbial improved oil recovering, biosensors and bioengineering and continuing modifications. Kuznetsov [24] presented the applications of nanofluid in presence of gyrotactic microorganisms.

Kairi et al. [25] examined the solutal Marangoni effect in swimming of motile microorganisms over an inclination stretched surface. Chen et al. [26] evaluated the thermal aspects of bioconvection. Rao et al. [27] established the computational model for Darcy free convective of nanofluid with motile microorganism over an isothermally vertical cone with porous space. Chu et al. [28] discussed a two-dimensional viscous containing gyrotactic microorganisms. Zadeh et al. [29] researched on the mathematical modeling of nanofluid with bioconvection applications over a vertical stretched surface under the influence of motile gyrotactic microorganisms. The thermal assessment of thixotropic nanoparticles with gyrotactic motile microorganisms and activation energy was scrutinized by Khan et al. [30]. Haq et al. [31] performed the simulations for bioconvection aspects of Williamson nanofluid in presence of activa-

tion energy. Shah et al. [32] scrutinized the bioconvection effects in water-based nanoparticles with single-wall and multi-wall carbon nanotubes over a vertical cone. Khan et al. [33] described the thermal radiative analysis for ferromagnetic Jeffrey nanofluid with gyrotactic microorganisms and electromagnetic dipole. Sajid et al. [34] conducted the double-diffusion bioconvection flow of tangential hyperbolic nanoparticles over stretched surface. Some more inspired investigations on this topic are referred to the refs. [35–40].

This investigation deals with the stagnation point flow of micropolar nanofluid containing gyrotactic microorganism confined by off centered rotating disk with Darcy resistance. The flow problem is modified by utilizing the activation energy, thermal radiation and magnetic force. The pioneer work on stagnation point flow of viscous fluid over an off centered rotating disk was directed by Wang [41]. Khan et al. [42] extended the Wang’s problem for micropolar fluid in presence of Darcy resistance. However, the stagnation point flow of micropolar nanofluid with gyrotactic microorganisms in presence of activation energy and thermal radiation has not been investigated yet. With these motivations, this communication aims to fulfill this research gap. The modeled flow problem for non-Newtonian fluid convinced many applications in thermal engineering, solar receiver devices, cooling and heating processes, catalytic reactors, thermodynamics processes, energy storage units, fission and fusion reactions, ceramic processing etc. Similarly, the bioconvection flow of nanofluid reflected importance in biotechnology, bio-engineering, enzymes, bacteria, biofuels etc. The numerical technique with excellent accuracy is developed to present the numerical simulations. The physical review of flow parameters is underlined with help of graphs and tables.

2. Mathematical formulation

The incompressible stagnation point flow of bio-convective micropolar nanofluid past an off centered rotating disk is con-

sidered. The consequence of thermal radiation in temperature equation is taken into account. The disk is rotatable with angular velocity ω . The velocity components u_1 , v_1 and w_1 are taken in x –, y – and z –directions, respectively as shown in Fig. 1. The temperature at surface of the disk is denoted by T_w while T_∞ is free stream temperature. Furthermore C_w and C_∞ signifies surface concentration and ambient concentration, respectively. Moreover, N_w and N_∞ represents the microorganisms at surface and ambient microorganism, respectively. The three-dimensional rotating disk is assumes to be porous. The thermal radiation features with nonlinear relations and activation energy are also taken into consideration. The modeled problem is solved numerically by incorporating the shooting scheme. The governing equations for micropolar nanofluid with bioconvection phenomenon are represented as [41]:

$$\frac{\partial u_1}{\partial x} + \frac{\partial v_1}{\partial y} + \frac{\partial w_1}{\partial z} = 0, \tag{1}$$

$$u_1 \frac{\partial u_1}{\partial x} + v_1 \frac{\partial u_1}{\partial y} + w_1 \frac{\partial u_1}{\partial z} = -\frac{1}{\rho} \frac{\partial p}{\partial x} + \left(\frac{\mu+\kappa}{\rho}\right) \left(\frac{\partial^2 u_1}{\partial x^2} + \frac{\partial^2 u_1}{\partial y^2} + \frac{\partial^2 u_1}{\partial z^2}\right) + \frac{\kappa}{\rho} \frac{\partial N_2}{\partial z} - \frac{\varphi}{k_1} \left(\frac{\mu+\kappa}{\rho}\right) u_1 + \frac{1}{\rho_f} \left[\begin{array}{l} (1 - C_f) \rho_f \beta^{**} g^* (T - T_\infty) \\ -(\rho_p - \rho_f) g^* (C - C_\infty) \\ -(N - N_\infty) g^* \gamma (\rho_m - \rho_f) \end{array} \right], \tag{2}$$

$$u_1 \frac{\partial v_1}{\partial x} + v_1 \frac{\partial v_1}{\partial y} + w_1 \frac{\partial v_1}{\partial z} = -\frac{1}{\rho} \frac{\partial p}{\partial y} + \left(\frac{\mu+\kappa}{\rho}\right) \left(\frac{\partial^2 v_1}{\partial x^2} + \frac{\partial^2 v_1}{\partial y^2} + \frac{\partial^2 v_1}{\partial z^2}\right) - \frac{\kappa}{\rho} \frac{\partial N_1}{\partial z} - \frac{\varphi}{k_1} \left(\frac{\mu+\kappa}{\rho}\right) v_1, \tag{3}$$

$$u_1 \frac{\partial w_1}{\partial x} + v_1 \frac{\partial w_1}{\partial y} + w_1 \frac{\partial w_1}{\partial z} = -\frac{1}{\rho} \frac{\partial p}{\partial z} + \left(\frac{\mu+\kappa}{\rho}\right) \left(\frac{\partial^2 w_1}{\partial x^2} + \frac{\partial^2 w_1}{\partial y^2} + \frac{\partial^2 w_1}{\partial z^2}\right) + \frac{\kappa}{\rho} \left(\frac{\partial N_2}{\partial x} + \frac{\partial N_1}{\partial y}\right), \tag{4}$$

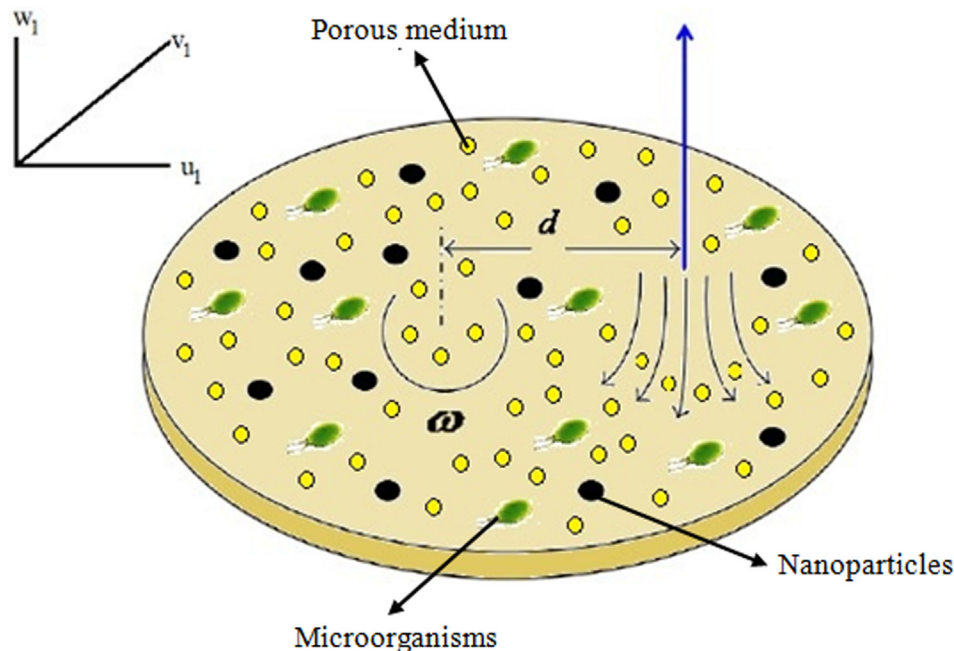


Fig. 1 Physical view of model.

$$\begin{aligned} & \rho j \left(u_1 \frac{\partial N_1}{\partial x} + v_1 \frac{\partial N_1}{\partial y} + w_1 \frac{\partial N_1}{\partial z} \right) \\ &= \gamma_1 \left(\frac{\partial^2 N_1}{\partial x^2} + \frac{\partial^2 N_1}{\partial y^2} + \frac{\partial^2 N_1}{\partial z^2} \right) - \kappa \left(2N_1 + \frac{\partial w_1}{\partial y} - \frac{\partial v_1}{\partial z} \right), \end{aligned} \quad (5)$$

$$\begin{aligned} & \rho j \left(u_1 \frac{\partial N_2}{\partial x} + v_1 \frac{\partial N_2}{\partial y} + w_1 \frac{\partial N_2}{\partial z} \right) \\ &= \gamma_1 \left(\frac{\partial^2 N_2}{\partial x^2} + \frac{\partial^2 N_2}{\partial y^2} + \frac{\partial^2 N_2}{\partial z^2} \right) - \kappa \left(2N_2 + \frac{\partial u_1}{\partial z} - \frac{\partial w_1}{\partial x} \right), \end{aligned} \quad (6)$$

$$\begin{aligned} & u_1 \frac{\partial T}{\partial x} + v_1 \frac{\partial T}{\partial y} + w_1 \frac{\partial T}{\partial z} = \alpha_1 \frac{\partial^2 T}{\partial z^2} \\ &+ \tau \left(D_B \frac{\partial T}{\partial z} \frac{\partial C}{\partial z} + \frac{D_T}{T_\infty} \left(\frac{\partial T}{\partial z} \right)^2 \right) - \frac{16\sigma^*}{3(\rho c)k^*} \frac{\partial}{\partial z} \left(T^3 \frac{\partial T}{\partial z} \right), \end{aligned} \quad (7)$$

$$\begin{aligned} & u_1 \frac{\partial C}{\partial x} + v_1 \frac{\partial C}{\partial y} + w_1 \frac{\partial C}{\partial z} = D_B \left(\frac{\partial^2 C}{\partial z^2} \right) + \frac{D_T}{T_\infty} \left(\frac{\partial^2 T}{\partial z^2} \right) \\ &- Kr^2 (C - C_\infty) (T/T_\infty)^{n_0} \exp(-Ea/T\bar{k}_i), \end{aligned} \quad (8)$$

$$\begin{aligned} & u_1 \frac{\partial N}{\partial x} + v_1 \frac{\partial N}{\partial y} + w_1 \frac{\partial N}{\partial z} + \left[\frac{\partial}{\partial z} \left(N \frac{\partial C}{\partial z} \right) \right] \frac{bW_c}{(C_w - C_\infty)} \\ &= D_m \frac{\partial}{\partial z} \left(\frac{\partial N}{\partial z} \right), \end{aligned} \quad (9)$$

where u_1, v_1 and w_1 represents the velocity components along x, y and z directions, respectively. Moreover, ρ denotes the density of fluid, ρ_m signifies microorganism density number, g^* be the gravity, j is the micro-inertia, α_1 examine the thermal diffusivity, D_B and D_T are the Brownian and thermophoresis coefficient, τ denotes the heat capacities ratio, mean absorption coefficient is symbolized by k^* , σ^* denotes Stephan-Boltzmann, D_m be the microorganism coefficient, W_c be cell swimming speed, b be the chemotaxis constant, the porosity of the permeable medium is denoted by φ , permeability symbolized by k_1 , (N_1, N_2) displays the components for microrotation vector N regular to the plane xz and yz etc, the above partial differential equations solved by using the suitable boundary conditions [41,42]:

$$\begin{aligned} & u_1 = -\omega y, \quad v_1 = \omega(x-d), \quad w_1 = w_0, \\ & N_1 = n \frac{\partial v_1}{\partial z}, \quad N_2 = -n \frac{\partial u_1}{\partial z}, \quad -k \frac{\partial T}{\partial z} = h_f (T_f - T), \\ & D_B \frac{\partial C}{\partial z} + \frac{D_T}{T_\infty} \frac{\partial T}{\partial z} = 0, \quad N = N_f \quad \text{at } z \rightarrow 0 \end{aligned} \quad (10)$$

$$\begin{aligned} & u_1 = ax, \quad v_1 = ay, \quad w_1 = -2az, \quad N_1 \rightarrow 0, \quad N_2 \rightarrow 0, \\ & T \rightarrow T_\infty, \quad C \rightarrow C_\infty, \quad N \rightarrow N_\infty, \quad \text{as } z \rightarrow \infty. \end{aligned} \quad (11)$$

It is remarked that boundary conditions at infinity ($u_1 = ax, v_1 = ay, w_1 = -2az$) corresponds to the potential flow, where a reflects the strength of the stagnation flow. The boundary conditions ($u_1 = -\omega y, v_1 = \omega(x-d), w_1 = w_0$) are assumed at the disk surface. Moreover, the strength of the stagnation fluid flow characterized by a , boundary constant represented by n like that $0 \leq n \leq 1$. Guram and Smith [43] explore the case $n = 0$, in which they identified as physically powerful nanoparticles concentration; the microelements near to a wall are not capable to revolve, close the wall $N = 0$. The smaller nanoparticles concentrations are experimental in casing $n = \frac{1}{2}$ owing to the vanishing of the anti-symmetric component for the stress tensor [44]. In case $n = 1$ was projected by Peddieson [45] where the investigation of the unstable boundary layer fluid flows.

Let us introduce appropriate variables [41,42]:

$$\begin{aligned} & u_1 = axf'(\zeta) - \omega yg(\zeta) + dok(\zeta), \\ & v_1 = ayf'(\zeta) + \omega xg(\zeta) + doh(\zeta), \\ & w_1 = -2\sqrt{av}f(\zeta), \quad \zeta = z\sqrt{\frac{a}{v}}, \quad N_1 = ay\sqrt{\frac{a}{v}}G(\zeta), \\ & N_2 = ax\sqrt{\frac{a}{v}}F(\zeta), \quad \theta(\zeta) = T - T_\infty/T_f - T_\infty, \\ & \phi(\zeta) = C - C_\infty/C_f - C_\infty, \quad \chi(\zeta) = N - N_\infty/N_f - N_\infty. \end{aligned} \quad (12)$$

Utilizing the above appropriate variables in Eqs. (1)–(9), the continuity equation is satisfied while remaining flow equations get following dimensionless forms [42]:

$$\begin{aligned} & (1+d1)(f''' - wf') + d1F' + 2ff'' - f^2 + \alpha^2 g^2 + 1 \\ &+ \lambda(\theta - Nr\phi - Nc\chi) = 0, \end{aligned} \quad (13)$$

$$(1+d1)(g'' - wg) + 2g'f - 2gf' = 0, \quad (14)$$

$$(1+d1)(k'' - wk) + \alpha gh - f'k + 2fk' = 0, \quad (15)$$

$$(1+d1)(h'' - wh) - \alpha gk - f'h + 2fh' = 0, \quad (16)$$

$$F'' - 2d2F - d3Ff' + 2d3Ff - d2f'' = 0, \quad (17)$$

$$G'' - 2d2G - d3Gf' + 2d3Gf - d2f'' = 0, \quad (18)$$

$$\left(1 + \frac{4}{3} Rd \right) \theta'' + Prf\theta' + PrNb\theta'\phi' + PrNt(\theta')^2 = 0, \quad (19)$$

$$\phi'' + LePrf\phi' + \frac{Nt}{Nb}\theta'' - LePr\delta^* \phi(1 + \delta_1\theta)^{n_0} \exp(-E/(1 + \delta_1\theta)) = 0, \quad (20)$$

$$\chi'' + Lbf\chi' - Pe[\phi''(\chi + \delta) + \chi'\phi'] = 0. \quad (21)$$

with boundary conditions

$$\begin{aligned} & f(0) = A, \quad f'(0) = 0, \quad g(0) = 1, \quad k(0) = 0, \quad h(0) = 1, \\ & F(0) = -f''(0), \quad G(0) = f''(0), \quad \theta'(0) = -Bi(1 - \theta(0)), \\ & \phi'(0) + Nt/Nb\theta'(0) = 0, \quad \chi(0) = 1, \\ & f'(\infty) \rightarrow 1, \quad g(\infty) \rightarrow 0, \quad k(\infty) \rightarrow 0, \quad h(\infty) \rightarrow 0, \\ & F(\infty) \rightarrow 0, \quad G(\infty) \rightarrow 0, \quad \theta(\infty) \rightarrow 0, \quad \phi(\infty) \rightarrow 0, \quad \chi(\infty) \rightarrow 0. \end{aligned} \quad (22)$$

where $\alpha = \frac{\omega}{a}$ represent the dimensionless rotation parameter, material parameter expressed by $d1 = \frac{\kappa}{\mu}$, spin gradient viscosity symbolized by $d2 = \frac{\kappa v}{\sigma_1}$, micro inertia density denoted by $d3 = \frac{\rho v}{\gamma_1}$, porosity parameter characterized by $w = \frac{v\varphi}{ak_1}$, parameter, $\alpha = \frac{\beta^* g^*(1-C_\infty)(T_f-T_\infty)}{aw_w}$ be the mixed convection parameter, $Nr = \frac{(\rho_p - \rho_f)(C_w - C_\infty)}{\rho_f(1-C_\infty)(T_w - T_\infty)\beta^*}$ is Buoyancy ratio parameter, the Bioconvection Rayleigh number is defined by $Nc = \frac{\gamma^*(\rho_m - \rho_f)(N_f - N_\infty)}{\rho_f(1-C_\infty)(T_f - T_\infty)\beta^*}$, the Brownian diffusion parameters characterized by $Nb = \frac{\tau D_B}{v}(C_f - C_\infty)$, $Nt = \frac{\tau D_T}{vT_\infty}(T_f - T_\infty)$ denotes the thermophoresis, $Rd = 4\sigma^*T_\infty^3/Kk^*$ be the thermal radiation, $E = E_a/T_\infty \bar{k}_i$, $\delta_1 = (T_w - T_\infty)/T_\infty$, are activation and temperature difference parameter, $Pr = \frac{\rho_0}{v}$ be the Prandtl number, Lewis number is denoted by $Lb = \frac{\rho_0}{D_B}$, bioconvection Lewis number is denoted by $Lb = \frac{\rho_0}{D_m}$, Peclet number is illustrated by $Pe = \frac{bW_c}{D_m}$, the microorganisms difference variable is

denoted by $\delta = \frac{N_{sc}}{N_f - N_{sc}}$, thermal Biot number $Bi = \frac{h_f}{k} \sqrt{\frac{a}{\nu}}$, $A = \frac{-w_0}{2\sqrt{av}}$ uniform injection generated by Eqs. (10, 12). Where S denoted the uniformed injection parameter $A > 0$. Computing the pressure p form Eq. (3), we get:

$$p = p_0 - \frac{1}{2} \rho a^2 (x^2 + y^2) - \rho \left(\frac{w^2}{2} - \left(\frac{\mu + \kappa}{\rho} \right) w_z \right), \quad (23)$$

where p_0 expressed the pressure at the origin. The shear stress over the off centered revolving disk of micropolar nanofluid in the permeable medium is as follows:

$$\tau_{xz} = \rho \left(\left(\frac{\mu + \kappa}{\rho} \right) \frac{\partial u}{\partial z} + \frac{\kappa}{\rho} N_2 \right) \Big|_{z=0},$$

$$\tau_{xz} = \rho a \sqrt{va} \left[\begin{array}{l} x(f''(0) + d1f''(0) + d1f'(0)) - \alpha y(g'(0) + d1g'(0)) \\ + d\alpha(k'(0) + d1k'(0)) \end{array} \right], \quad (24)$$

$$\tau_{yz} = \rho \left(\left(\frac{\mu + \kappa}{\rho} \right) \frac{\partial v}{\partial z} - \frac{\kappa}{\rho} N_1 \right) \Big|_{z=0},$$

$$\tau_{yz} = \rho a \sqrt{va} \left[\begin{array}{l} y(f''(0) + d1f''(0) - d1G(0)) + \alpha x(g'(0) + d1g'(0)) \\ + d\alpha(h'(0) + d1h'(0)) \end{array} \right]. \quad (25)$$

The shear stress at the middle point is zero, the shear stress over the layer of the disk can be attained through Eqs. (24) and (25) to zero and resolve for (x, y) . the torque practiced through the disk with radius R is written as:

$$M = \int_0^R \int_0^{2\pi} (\tau_{yz} \cos\theta - \tau_{xz} \sin\theta) r^2 d\theta dr \quad (26)$$

Here (r, θ) represents the cylindrical coordinates, extra stress tensor demonstrated by τ_x, τ_{xz} and τ_{yz} components of the extra stress tensor that are (xz, yz) . While, $x = r \cos\theta - b$, the torque can be establish at:

$$M = \frac{\pi}{2} a \sqrt{av} \alpha R^4 (\rho g'(0) + d1g'(0)) \quad (27)$$

That is unchanged by the non-aligned disk.

3. Numerical method

The shooting scheme is used to integrate the nonlinear ordinary differential equations defined by Eqs. (13)–(21) with boundary conditions (22). Shooting method is more useful technique to solve the nonlinear higher order system of problem. The higher order differential equations are reduced to first order boundary problem by substitutions new variables:

Let

$$\begin{aligned} f &= p_1, f' = p_2, f'' = p_3, f''' = p'_3, \\ g &= p_4, g' = p_5, g'' = p'_5, k = p_6, k' = p_7, \\ k'' &= p'_7, h = p_8, h' = p_9, h'' = p'_9, F = p_{10}, \\ F' &= p_{11}, F'' = p'_{11}, G = p_{12}, G' = p_{13}, G'' = p'_{13}, \\ \theta &= p_{14}, \theta' = p_{15}, \theta'' = p'_{15}, \phi = p_{16}, \phi' = p_{17}, \phi'' = p'_{17}, \\ \chi &= p_{18}, \chi' = p_{19}, \chi'' = p'_{19}. \end{aligned} \quad (28)$$

$$p'_3 = \frac{(1+d1)wp_2 - d1p_{11} - 2p_1p_3 + p_2^2 - \alpha^2 p_4 - 1 - \lambda(p_{14} - Nr p_{16} - Nc p_{18})}{(1+d1)}, \quad (29)$$

$$p'_5 = \frac{(1+d1)wp_4 - 2p_5p_1 + 2p_4p_2}{(1+d1)} \quad (30)$$

$$p'_7 = \frac{(1+d1)wp_6 - \alpha p_4 p_8 + p_2 p_6 - 2p_1 p_7}{(1+d1)} \quad (31)$$

$$p'_9 = \frac{(1+d1)wp_8 + \alpha p_4 p_6 + p_2 p_8 - 2p_1 p_9}{(1+d1)}, \quad (32)$$

$$p'_{11} = 2d2p_{10} + d3p_{10}p_2 - 2d3p_{11}p_1 + d2p_3, \quad (33)$$

$$p'_{13} = 2d2p_{12} + d3p_{12}p_2 - 2d3p_{13}p_1 + d2p_3 \quad (34)$$

$$p'_{15} = \frac{-Pr p_1 p_{15} - Pr Nb p_{15} p_{17} - Pr Nt (p_{15})^2}{(1 + \frac{4}{3} Rd)}, \quad (35)$$

$$p'_{17} = -Le Pr p_1 p_{17} - \frac{Nt}{Nb} p'_{15} + Le Pr \delta^* p_{16} (1 + \delta_1 p_{14})^{n_0} \exp(-E/(1 + \delta_1 p_{14})), \quad (36)$$

$$p'_{19} = -Lb p_1 p_{19} + Pe [p'_{17} (p_{18} + \delta) + p_{19} p_{17}]. \quad (37)$$

With

$$\begin{aligned} p_1(0) &= A, \quad p_2(0) = 0, \quad p_4(0) = 1, \quad p_6(0) = 0, \quad p_8(0) = 1, \\ p_{10}(0) &= -p_3(0), \quad p_{12}(0) = p_3(0), \quad p_{15}(0) = -Bi(1 - p_{14}(0)), \\ p_{17}(0) &+ Nt/Nb p_{15}(0) = 0, \quad p_{18}(0) = 1, \\ p_2(\infty) &= 1, \quad p_4(\infty) = 0, \quad p_6(\infty) = 0, \quad p_8(\infty) = 0, \\ p_{10}(\infty) &= 0, \quad p_{12}(\infty) = 0, \quad p_{14}(\infty) = 0, \quad p_{16}(\infty) = 0, \quad p_{18}(\infty) = 0. \end{aligned} \quad (38)$$

4. Results and discussion

This section aims to investigate the features of velocity functions (f, g, k, h) , microrotation fields (F, G) , temperature field θ , concentration profile ϕ and microorganism's field χ through Figs. 2–15. Fig. 2 portrays the impact of suction/injection parameter A and dimensionless rotation parameter α on radial velocity field f' . Interesting result to observe here is that radial velocity f' is reduced for larger variations of suction/injection parameter A and dimensionless rotation parameter α . In Fig. 3 the effect of buoyancy ratio parameter Nr and bioconvection Rayleigh number Nc on the radial velocity function f' is captured. It is evident that an enlargement in buoyancy ratio parameter Nc corresponds to decrement in radial function f' . Radial velocity f' is significantly reduced with larger bioconvection Rayleigh number Nc . The properties of radial velocity field f' against material parameter $d1$ and porosity parameter w is shown in Fig. 4. It is observed that material parameter $d1$ increases with reduce the radial velocity f' of fluid. It is noted that radial function f' is decline for larger variation of porosity parameter w . Fig. 5 examines the aspects of porosity parameter w and suction/injection parameter A on azimuthal velocity field g . Here it is noted that azimuthal function g is retarded down due to increasing values of porosity parameter w and suction/injection parameter A . Behavior of material parameter $d1$ and porosity parameter w on induced velocity distribution k is demonstrated in Fig. 6. Here profile of induced velocity k has opposite behavior for both material parameter $d1$ and porosity parameter w . Fig. 7 illustrates the evolution of induced velocity k for larger variations of dimensionless rotation parameter α and suction/injection parameter A . Induced velocity field k curves reveals that by enlarging

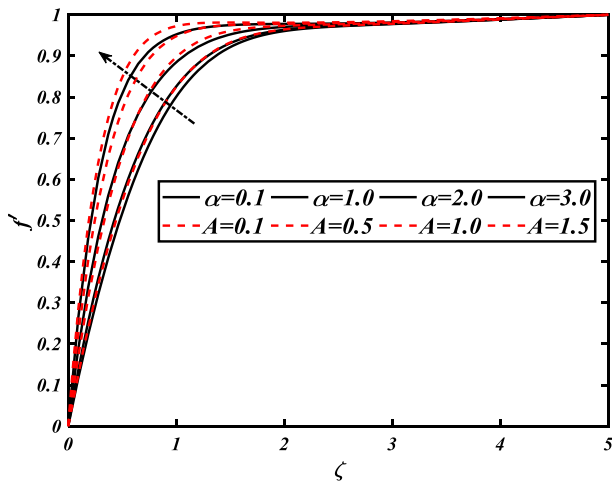


Fig. 2 Variability of f' through α & A .

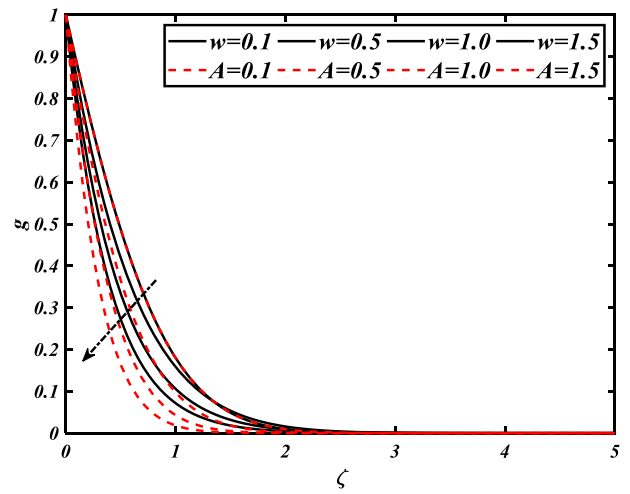


Fig. 5 Variability of g through w & A .

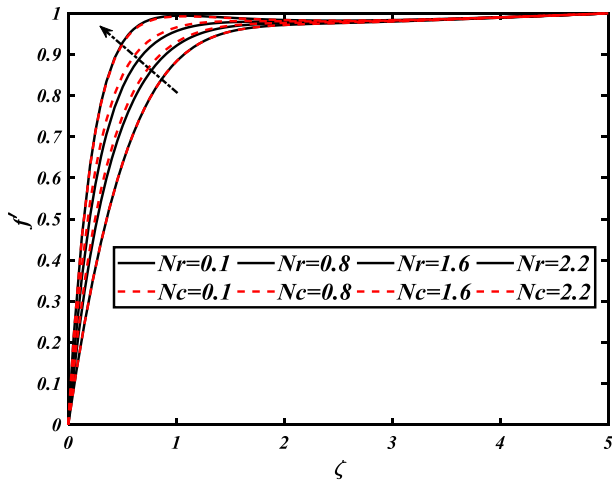


Fig. 3 Variability of f' through Nr & Nc .

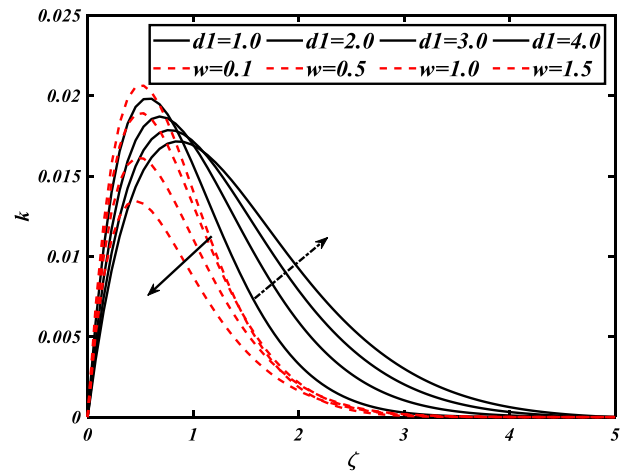


Fig. 6 Variability of k through $d1$ & w .

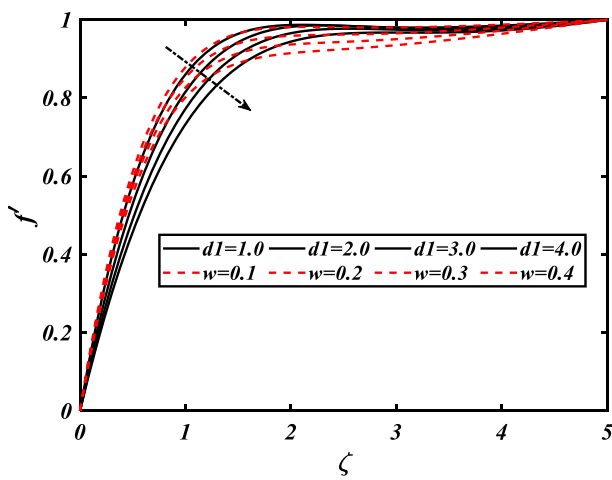


Fig. 4 Variability of f' through $d1$ & w .

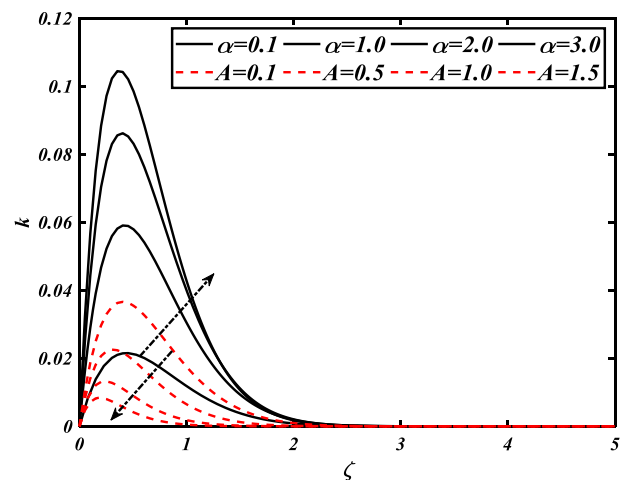


Fig. 7 Variability of k through α & A .

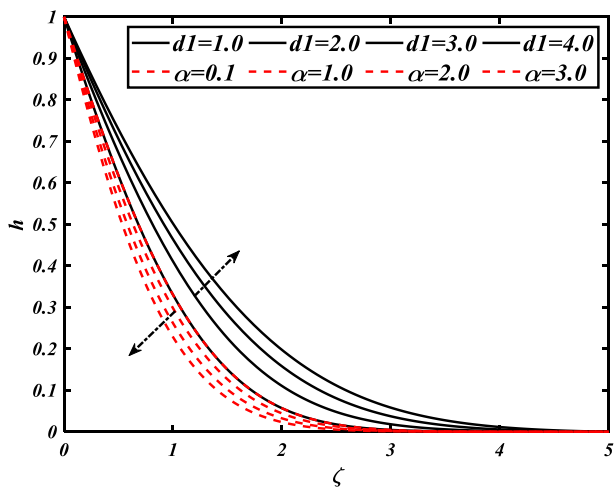


Fig. 8 Variability of h through $d1$ & A .

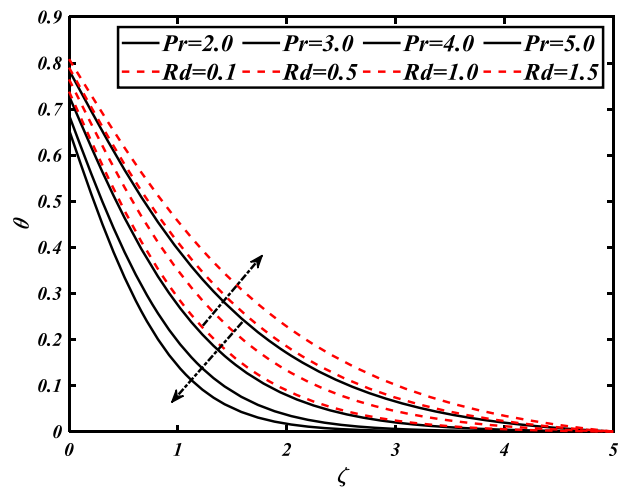


Fig. 11 Variability of θ through Pr & Rd

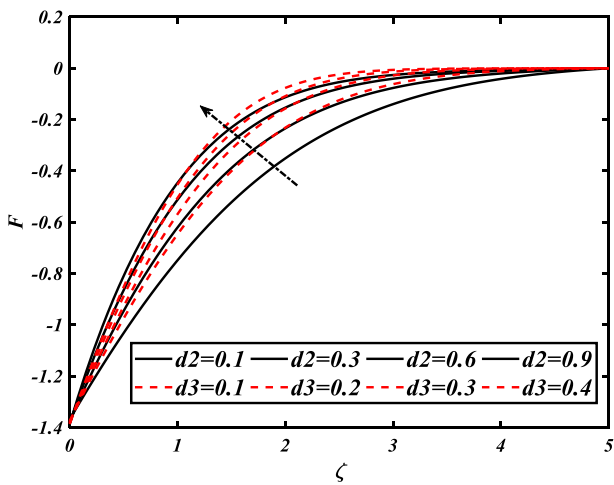


Fig. 9 Variability of F through $d2$ & $d3$.

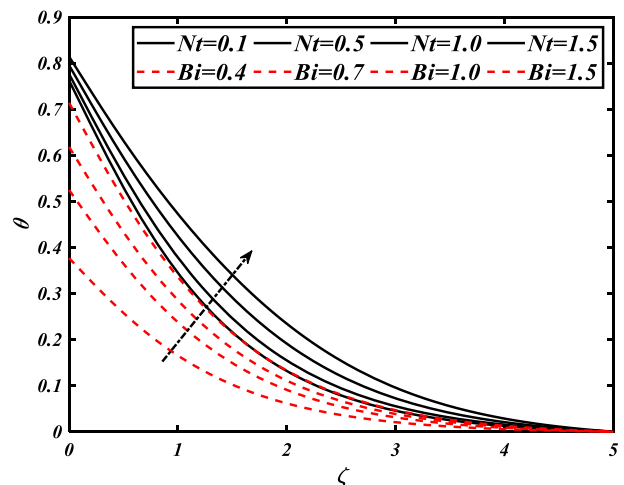


Fig. 12 Variability of θ through Nt & Bi .

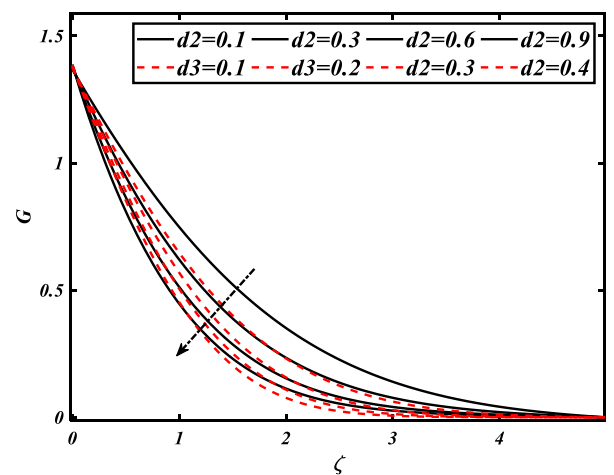


Fig. 10 Variability of G through $d2$ & $d3$

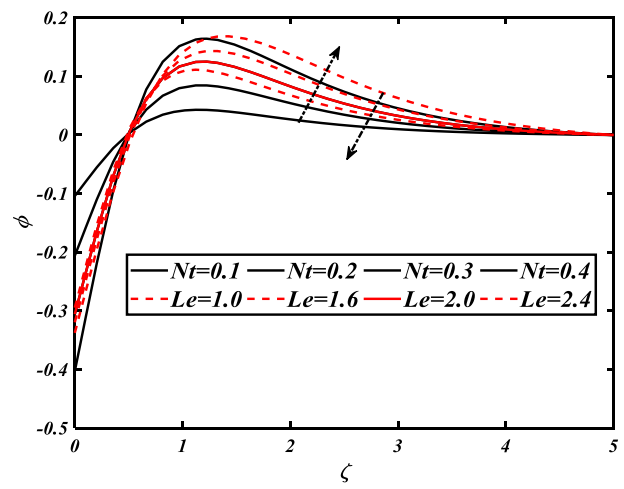


Fig. 13 Variability of ϕ through Nt & Le .

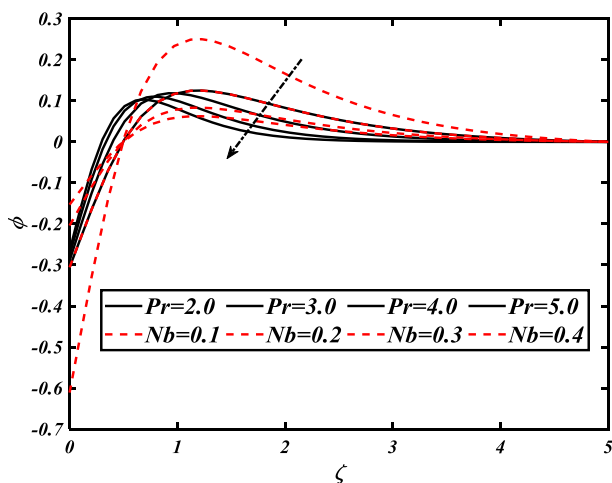


Fig. 14 Variability of ϕ through Pr & Nb .

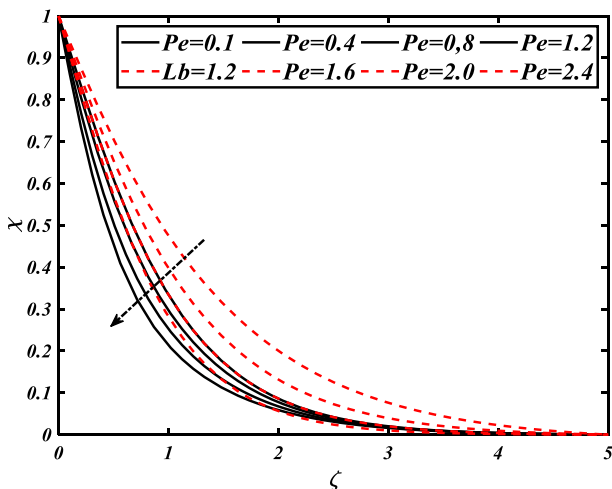


Fig. 15 Variability of χ through Pe & Lb .

dimensionless rotation parameter α the induced velocity function k is boosted. It is noted that induced velocity profile k is declines with larger suction/injection parameter A . Fig. 8 is designed to illustrate the effect of material parameter $d1$ and dimensionless rotation parameter α on component of velocity h . The velocity h is rises for higher material parameter $d1$ while reduced with dimensionless rotation parameter α .

The impact of spin gradient viscosity parameter $d2$ and micro-inertia density parameter $d3$ on microrotation field F is shown in Fig. 9. The microrotation profile F is manifested with higher amount of spin gradient viscosity parameter $d2$ and micro-inertia density parameter $d3$. The trend of spin gradient viscosity parameter $d2$ and micro-inertia density parameter $d3$ against microrotation component G is demonstrated through Fig. 10. It is noted that microrotation component G is declines for larger spin gradient viscosity parameter $d2$. From this figure we noted that microrotation field G is declines for increases micro-inertia density parameter $d3$.

Fig. 11 depicts the salient features of Prandtl number Pr and thermal radiation parameter Rd on temperature distribution θ . Temperature profile θ considerably improved with enhancing radiation parameter Rd . From this analysis we analyzed that temperature θ is declined for larger estimation of Prandtl number Pr . Fig. 12 presents the impact of thermophoresis parameter Nt and thermal Biot number Bi on thermal field of species θ . Temperature distribution θ is also improved with growing thermophoresis parameter Nt . It is noted that heat of fluid θ is rises for larger thermal Biot number Bi .

Fig. 13 presents the concentration of species ϕ for various values of thermophoresis parameter Nt and Lewis number Le . It is scrutinized that concentration field ϕ is exaggerates for larger variation of thermophoresis parameter Nt . Here, it can be found that concentration ϕ is decays for larger estimation of Lewis number Le . Behavior of Prandtl number Pr and Brownian motion parameter Nb for volumetric concentration of nanoparticles ϕ in considered in Fig. 14. Larger Brownian motion parameter Nb decays the concentration field ϕ . It is seen that concentration of nanoparticles ϕ is diminishes for larger estimation of Prandtl number Pr .

Fig. 15 examines the effect of Peclet number Pe and bioconvection Lewis number Lb on microorganism's field χ . It is observed that microorganism field χ is reduces with increases Peclet number Pe . From this figure it can be found that microorganism distribution χ is decays for larger variations of bioconvection Lewis number Lb .

Tables 1–4 presents the numerical data for local skin friction coefficients, local Nusselt number, local Sherwood number and local microorganism's density number against different values of parameters. Table 1 is designed to examine the numerical data of local skin friction coefficients for different values of parameters. From this table we observed that a local skin friction coefficients increases for larger estimation of mixed convection parameter and spin-gradient viscosity. It is concluded from Table 2, that heat transfer rate (Nusselt number) reduce with increase in thermophoresis parameter, thermal radiation parameter and porosity parameter. Variations of the local Sherwood number for the prominent parameters are recorded in Table 3. Here local Sherwood number is rises for larger values of Brownian motion parameter and Prandtl number. it is founded from Table 4, that local microorganisms density number decreases for larger variation of Peclet number and bioconvection Lewis number.

5. Conclusions

The stagnation point flow of micropolar nanofluid containing motile microorganisms is numerically analyzed over an off centered rotating disk. The applications of activation energy and thermal radiation are also utilized. The numerical solution with shooting technique is presented. Some significant results are summarized below:

- The variability of radial velocity field enhancing for enlarging values of suction/injection parameter and mixed convection parameter.

Table 1 Numerical result for $f''(0)$, $-g'(0)$, $k'(0)$ and $-h'(0)$ for prominent parameters.

λ	$d1$	$d2$	$d3$	A	Nc	Skin friction coefficient			
						$f''(0)$	$-g'(0)$	$k'(0)$	$-h'(0)$
0.5	1.0	0.1	0.1	0.1	0.5	1.1908	0.9066	0.0872	0.8126
1.5						1.6055	0.9567	0.2484	0.8647
2.0						1.9409	0.9933	0.3188	0.9024
1.0	2.0	0.1	0.1	0.1	0.5	1.2141	0.7828	0.1345	0.7055
	3.0					1.1164	0.6968	0.1134	0.6301
	4.0					1.0404	0.6384	0.0991	0.5794
1.0	1.0	0.5	0.1	0.1	0.5	1.4472	0.9463	0.1693	0.8409
		1.0				1.5071	0.9606	0.1688	0.8440
		1.5				1.5446	0.9424	0.1687	0.8453
1.0	1.0	0.1	0.5	0.1	0.5	1.4850	0.9421	0.1684	0.8455
			1.0			1.5661	0.9476	0.1678	0.8493
			1.5			1.6173	0.9494	0.1656	0.8504
1.0	1.0	0.1	0.1	0.2	0.5	1.4336	0.9951	0.1647	0.9010
				0.4		1.6106	1.1380	0.1531	1.0427
				0.8		2.0101	1.4441	0.1323	1.3490
1.0	1.0	0.1	0.1	0.1	0.4	1.4533	0.9878	0.1455	0.9125
					0.8	1.6097	1.1435	0.1643	1.0678
					1.6	1.7045	1.4560	0.1699	1.3645

Table 2 Numerical result for $-\theta'(0)$ against prominent parameters.

Pr	Nt	λ	Rd	$d1$	$d2$	$d3$	w	Bi	$-\theta'(0)$
2.5	0.3	1.0	0.6	1.0	0.1	0.1	0.1	2.0	0.5457
3.5									0.6028
4.5									0.6466
2.0	0.1	1.0	0.6	1.0	0.1	0.1	0.1	2.0	0.5175
	0.5								0.5008
	1.0								0.4792
2.0	0.3	0.5	0.6	1.0	0.1	0.1	0.1	2.0	0.5013
		1.5							0.5210
		2.0							0.5351
2.0	0.3	1.0	0.4	1.0	0.1	0.1	0.1	2.0	0.5321
			0.8						0.4897
			1.6						0.4324
2.0	0.3	1.0	0.6	2.0	0.1	0.1	0.1	2.0	0.5014
				3.0					0.4945
				4.0					0.4883
2.0	0.3	1.0	0.6	1.0	0.5	0.1	0.1	2.0	0.5126
					1.0				0.5139
					1.5				0.5144
2.0	0.3	1.0	0.6	1.0	0.1	0.5	0.1	2.0	0.5148
						1.0			0.5163
						1.5			0.5165
2.0	0.3	1.0	0.6	1.0	0.1	0.1	0.2	2.0	0.4986
							0.4		0.4781
							0.8		0.4406
2.0	0.3	1.0	0.6	1.0	0.1	0.1	0.1	2.5	0.5357
								3.0	0.5549
								3.5	0.5694

- Radial velocity field via material parameter and porosity parameter is reduced.
- Induced velocity component is boosted up with larger material parameter.
- The microrotation component is rises for larger spin gradient viscosity parameter and micro-inertia density parameter.
- Larger thermal Biot number enhances the temperature distribution.

Table 3 Numerical result for $-\phi'(0)$ against prominent parameters.

<i>Pr</i>	<i>Nt</i>	λ	<i>Nb</i>	<i>d1</i>	<i>d2</i>	<i>d3</i>	<i>w</i>	<i>Le</i>	$-\phi'(0)$
2.5	0.3	1.0	0.2	1.0	0.1	0.1	0.1	2.0	0.8185
3.5									0.9042
4.5									0.9698
2.0	0.1	1.0	0.2	1.0	0.1	0.1	0.1	2.0	0.2588
	0.5								1.2520
	1.0								2.3960
2.0	0.3	0.5	0.2	1.0	0.1	0.1	0.1	2.0	0.7519
		1.5							0.7815
		2.0							0.8026
2.0	0.3	1.0	0.1	1.0	0.1	0.1	0.1	2.0	1.5777
			0.5						0.3055
			1.0						0.1528
2.0	0.3	1.0	0.2	2.0	0.1	0.1	0.1	2.0	0.7521
				3.0					0.7418
				4.0					0.7325
2.0	0.3	1.0	0.2	1.0	0.5	0.1	0.1	2.0	0.7689
					1.0				0.7709
					1.5				0.7715
2.0	0.3	1.0	0.2	1.0	0.1	0.5	0.1	2.0	0.7722
						1.0			0.7744
						1.5			0.7748
2.0	0.3	1.0	0.2	1.0	0.1	0.1	0.2	2.0	0.7479
							0.4		0.7171
							0.8		0.6609
2.0	0.3	1.0	0.2	1.0	0.1	0.1	0.1	2.2	0.7254
								3.5	0.7460
								2.8	0.7770

Table 4 Numerical result for $-\chi'(0)$ against prominent parameters.

λ	<i>d1</i>	<i>d2</i>	<i>d3</i>	<i>A</i>	<i>Pe</i>	<i>Lb</i>	$-\chi'(0)$
0.5	1.0	0.1	0.1	0.1	0.1	2.0	0.8683
1.5							0.9147
2.0							0.9485
1.0	2.0	0.1	0.1	0.1	0.1	2.0	0.8688
	3.0						0.8533
	4.0						0.8397
1.0	1.0	0.5	0.1	0.1	0.1	2.0	0.8957
		1.0					0.8995
		1.5					0.9010
1.0	1.0	0.1	0.5	0.1	0.1	2.0	0.9011
			1.0				0.9058
			1.5				0.9072
1.0	1.0	0.1	0.1	0.2	0.1	2.0	1.0175
				0.4			1.2949
				0.8			1.8934
1.0	1.0	0.1	0.1	0.1	0.4	2.0	0.9205
					0.8		0.9667
					1.2		1.0146
1.0	1.0	0.1	0.1	0.1	0.1	4.0	1.2409
						5.0	1.3900
						6.0	1.5289

- Concentration of species rises for thermophoresis parameter.
- Larger Prandtl number decline the concentration of nanoparticles.
- A microorganism field is a decreasing function of Peclet number.

Declaration of Competing Interest

The authors declare that they have no known competing financial interests or personal relationships that could have appeared to influence the work reported in this paper.

References

- [1] S.U.S. Choi, D.A. Singer, H.P. Wang, Developments and applications of non-Newtonian flows, *ASME Fed.* 66 (1995) 99–105.
- [2] J. Buongiorno, Convective transport in nanofluids, *J. Heat Transf.* 128 (2006) 240–250.
- [3] J. Zhu, Y. Liu, J. Cao, Effects of second-order velocity slip and the different spherical nanoparticles on nanofluid flow, *Symmetry* 13 (1) (2021) 64.
- [4] B.P. Geridönmez, H.F. Öztöp, Effects of inlet velocity profiles of hybrid nanofluid flow on mixed convection through a backward facing step channel under partial magnetic field, *Chem. Phys.* 540 (2021) 111010.
- [5] B. Ali, R.A. Naqvi, A. Mariam, L. Ali, O.M. Aldossary, Finite element study for magnetohydrodynamic (MHD) tangent hyperbolic nanofluid flow over a faster/slower stretching wedge with activation energy, *Mathematics* 9 (1) (2021) 25.
- [6] A. Qureshi, M. Numerical Simulation of Heat Transfer Flow Subject to MHD of Williamson Nanofluid with Thermal Radiation. *Symmetry*, 13(1) (2021). 10.
- [7] R.P. Mehta, H.R. Kataria, Influence of magnetic field, thermal radiation and brownian motion on water-based composite nanofluid flow passing through a porous medium, *Int. J. Appl. Comput. Math.* 7 (1) (2021) 1–24.
- [8] Z. Poursharif, H. salarian, K. Javaherdeh, M. Eshagh Nimvari, Numerical simulation of heat transfer on nanofluid flow in an annular pipe with simultaneous embedding of porous discs and triangular fins, *J. Chin. Inst. Eng.* 44 (2) (2021) 158–169.
- [9] P. Sreedevi, P. Sudarsana Reddy, Heat and mass transfer analysis of MWCNT kerosene nanofluid flow over a wedge with thermal radiation, *Heat Transfer* 50 (1) (2021) 10–33.
- [10] E.E. Khalil, A. Kaood, Numerical investigation of thermal-hydraulic characteristics for turbulent nanofluid flow in various conical double pipe heat exchangers, *AIAA Scitech* (2021) 19–21.
- [11] T. Wen, L. Lu, S. Zhang, H. Zhong, Experimental study and CFD modelling on the thermal and flow behavior of EG/water ZnO nanofluid in multiport mini channels, *Appl. Therm. Eng.* 182 (2021) 116089, <https://doi.org/10.1016/j.applthermaleng.2020.116089>.
- [12] G. K. Ramesh; G. S. Roopa; Sabir Ali Shehzad; S. U. Khan, Interaction of Al₂O₃-Ag and Al₂O₃-Cu hybrid nanoparticles with water on convectively heated moving material, *Multidiscip. Model. Mater.* 016(6) (2020) 1651-1667.
- [13] S.U. Khan, H. Waqas, S.A. Shehzad, M. Imran, Theoretical analysis of tangent hyperbolic nanoparticles with combined electrical MHD, activation energy and Wu's slip features: a mathematical model, *Phys. Scr.* 94 (12) (2019) 125211.
- [14] T. Muhammad, H. Waqas, S.A. Khan, R. Ellahi, S.M. Sait, Significance of nonlinear thermal radiation in 3D Eyring-Powell nanofluid flow with Arrhenius activation energy, *J. Therm. Anal. Calorim.* 143 (2021) 929–944.
- [15] H. Waqas, M. Imran, S.U. Khan, S.A. Shehzad, M.A. Meraj, Slip flow of Maxwell viscoelasticity-based micropolar nanoparticles with porous medium: a numerical study, *Appl. Math. Mech.* 40 (9) (2019) 1255–1268.
- [16] S.U. Khan, I. Tlili, H. Waqas, M. Imran, Effects of nonlinear thermal radiation and activation energy on modified second-grade nanofluid with Cattaneo-Christov expressions, *J. Therm. Anal. Calorim.* 143 (2) (2021) 1175–1186.
- [17] A.A. Khan, S.R. Bukhari, M. Marin, R. Ellahi, Effects of chemical reaction on third-grade MHD fluid flow under the influence of heat and mass transfer with variable reactive index, *Heat Transfer Res.* 50 (11) (2019) 1061–1080.
- [18] A.R. Bestman, *Int. J. Energy Res.* 14 (1990) 389.
- [19] K. Gotoh, T. Mochizuki, T. Hojo, Y. Shibayama, Y. Kurokawa, E. Akiyama, N. Usami, Activation energy of hydrogen desorption from high-performance titanium oxide carrier-selective contacts with silicon oxide interlayers, *Curr. Appl. Phys.* 21 (2021) 36–42.
- [20] A.M. Alwatban, S.U. Khan, H. Waqas, I. Tlili, Interaction of Wu's slip features in bioconvection of Eyring-Powell nanoparticles with activation energy, *Processes* 7 (11) (2019) 859.
- [21] N.S. Khan, P. Kumam, P. Thounthong, Second law analysis with effects of Arrhenius activation energy and binary chemical reaction on nanofluid flow, *Sci. Rep.* 10 (1) (2020) 1–16.
- [22] M.M. Bhatti, M. Marin, A. Zeeshan, R. Ellahi, S.I. Abdelsalam, Swimming of motile gyrotactic microorganisms and nanoparticles in blood flow through anisotropically tapered arteries, *Front Phys.* 8 (2020) 1–12.
- [23] A.V. Kuznetsov, Nanofluid bioconvection in water-based suspensions containing nanoparticles and oxytactic microorganisms: oscillatory instability, *Nanoscale Res. Lett.* 6 (2011) Article number 100 (2011).
- [24] A.V. Kuznetsov, Bio-thermal convection induced by two different species of microorganisms, *Int. Commun. Heat Mass Transf.* 38 (2011) 548–553.
- [25] R.R. Kairi, S. Shaw, S. Roy, S. Raut, Thermosolutal marangoni impact on bioconvection in suspension of gyrotactic microorganisms over an inclined stretching sheet, *J. Heat Transf.* 143 (3) (2021).
- [26] K. Li, L. Chen, F. Zhu, Y. Huang, Thermal and mechanical analyses of compliant thermoelectric coils for flexible and bio-integrated devices, *J. Appl. Mech.* 88 (2) (2021).
- [27] M.V.S. Rao, K. Gangadhar, A.J. Chamkha, P. Surekha, Bioconvection in a convective nanofluid flow containing gyrotactic microorganisms over an isothermal vertical cone embedded in a porous surface with chemical reactive species, *Arab J Sci Eng* 46 (2021) 2493–2503.
- [28] Y.M. Chu, M.I. Khan, N.B. Khan, S. Kadry, S.U. Khan, I. Tlili, M.K. Nayak, Significance of activation energy, bio-convection and magnetohydrodynamic in flow of third grade fluid (non-Newtonian) towards stretched surface: A Buongiorno model analysis, *Int. Commun. Heat Mass.* 118 (2020) 104893.
- [29] S.M.H. Zadeh, S.A.M. Mehryan, M.A. Sheremet, M. Izadi, M. Ghodrati, Numerical study of mixed bio-convection associated with a micropolar fluid. *Therm. Sci. Eng. Prog.* (2020) 100539.
- [30] M.I. Khan, F. Haq, S.A. Khan, T. Hayat, M.I. Khan, Development of thixotropic nanomaterial in fluid flow with gyrotactic microorganisms, activation energy, mixed convection, *Comput. Methods Programs Biomed.* 187 (2020) 105186.
- [31] F. Haq, S. Kadry, Y.-M. Chu, M. Khan, M.I. Khan, Modeling and theoretical analysis of gyrotactic microorganisms in radiated nanomaterial Williamson fluid with activation energy, *J. Mater. Res. Technol.* 9 (5) (2020) 10468–10477.
- [32] Z. Shah, E. Alzahrani, M. Jawad, U. Khan, Microstructure and inertial characteristics of MHD suspended SWCNTs and MWCNTs based maxwell nanofluid flow with bio-convection and entropy generation past A permeable vertical cone, *Coatings* 10 (10) (2020) 998.
- [33] M. Ijaz, S. Nadeem, M. Ayub, S. Mansoor, Simulation of magnetic dipole on gyrotactic ferromagnetic fluid flow with nonlinear thermal radiation, *J. Therm. Anal. Calorim.* 143 (3) (2021) 2053–2067.
- [34] T. Sajid, M. Sagheer, S. Hussain, F. Shahzad, Impact of double-diffusive convection and motile gyrotactic microorganisms on magnetohydrodynamics bioconvection tangent hyperbolic nanofluid, *Open Phys.* 18 (1) (2020) 74–88.
- [35] H. Waqas, S.U. Khan, M. Hassan, M.M. Bhatti, M. Imran, Analysis on the bioconvection flow of modified second-grade nanofluid containing gyrotactic microorganisms and nanoparticles, *J. Mol. Liq.* 291 (2019) 111231.

- [36] M.I. Khan, F. Alzahrani, Free convection and radiation effects in nanofluid (Silicon dioxide and Molybdenum disulfide) with second order velocity slip, entropy generation, Darcy-Forchheimer porous medium, *Int. J. Hydrogen Energy* 46 (2021) 1362–1369.
- [37] M.I. Khan, F. Alzahrani, Cattaneo-Christov Double Diffusion (CCDD) and magnetized stagnation point flow of non-Newtonian fluid with internal resistance of particles, *Phys. Scr.* 95 (2020) 125002.
- [38] Z. Abdelmalek, S.U. Khan, H. Waqas, A.H. Nabwey, I. Tlili, Utilization of second order slip, activation energy and viscous dissipation consequences in thermally developed flow of third grade nanofluid with gyrotactic microorganisms, *Symmetry* 12 (2) (2020) 309.
- [39] M. Ijaz Khan, Faris Alzahrani, Nonlinear dissipative slip flow of Jeffrey nanomaterial towards a curved surface with entropy generation and activation energy, *Math. Comput. Simul* 185 (2021) 47–61.
- [40] M.I. Khan, Transportation of hybrid nanoparticles in forced convective Darcy-Forchheimer flow by a rotating disk, *Int. Commun. Heat Mass Transfer* 122 (2021) 105177.
- [41] C.Y. Wang, Off-centered stagnation flow towards a rotating disc, *Int. J. Eng. Sci.* 46 (4) (2008) 391–396.
- [42] N.A. Khan, S. Khan, A. Ara, Flow of micropolar fluid over an offcentered rotating disk with modified Darcy's law, *Propuls. Power Res.* 6 (4) (2017) 285–295.
- [43] G.S. Guram, A.C. Smith, Stagnation flows of micropolar fluids with strong and weak interactions, *Comput. Math. Appl.* 6 (2) (1980) 213–233.
- [44] G. Ahmadi, Self-similar solution of incompressible micropolar boundary layer flow over a semi-infinite plate, *Int. J. Eng. Sci.* 14 (7) (1976) 639–646.
- [45] J. Peddieson, An application of the micropolar fluid model to the calculation of turbulent shear flow, *Int. J. Eng. Sci.* 10 (1) (1972) 23–32.